

# Bulk Photovoltaics in Nanoscale Systems – Origin of Shift Currents in the Many-Body Picture

MingRui Lai

*Integrative Sciences and Engineering Programme,  
NUS Graduate School, National University of Singapore and  
Centre for Advanced 2D Materials, National University of Singapore, 6 Science Drive 2, Singapore 117546*

Fengyuan Xuan

*Department of Physics, National University of Singapore, 2 Science Drive 3, Singapore 117551 and  
Centre for Advanced 2D Materials, National University of Singapore, 6 Science Drive 2, Singapore 117546*

Su Ying Quek\*

*Department of Physics, National University of Singapore, 2 Science Drive 3, Singapore 117551  
Centre for Advanced 2D Materials, National University of Singapore, 6 Science Drive 2, Singapore 117546  
Integrative Sciences and Engineering Programme,  
NUS Graduate School, National University of Singapore and  
Department of Materials Science and Engineering, National University of Singapore  
(Dated: February 6, 2024)*

The shift current in bulk photovoltaics is commonly attributed to a shift in non-interacting charge centres. We show that the origin of shift currents in the many-body picture is fundamentally different. Here the shift current arises largely from a many-body shift vector that also involves shifts in charge centres, but these are associated with pairs of nearly-degenerate excitons overlapping in  $k$ -space. The shift current can thus be enhanced by nearly-degenerate, optically-active and tightly-bound excitons, spread out in  $k$ -space. *Ab initio* results are presented for BaTiO<sub>3</sub>, NbOCl<sub>2</sub> and MoS<sub>2</sub>.

The bulk photovoltaic effect is a strong contender for next-generation photovoltaic applications, being able to overcome the Shockley-Queisser limit on photovoltaic efficiencies [1]. The shift current is a major component of the bulk photovoltaic effect; it is a direct current that arises from a second-order nonlinear optical effect in crystals with broken inversion symmetry [2, 3]. The shift current is typically formulated within the independent particle approximation (IPA) where optical excitations are described by individual quasielectron and quasihole excitations. The IPA shift current is a weighted sum over positional shifts (“shift vector”) in the charge center from a valence ( $v$ ) to a conduction ( $c$ ) state at the same  $k$ -point [4, 5]. Early efforts in proposing designs of optimal materials for shift currents have relied on the IPA, even for low-dimensional materials [6].

It is known that photoexcitations in fact result in the formation of excitons–correlated electron-hole excitations–described using an effective two-body Bethe Salpeter Equation (BSE) approach [7]. The presence of such correlated electron-hole states is at odds with the idea of the shift vector as the positional shift in charge centre for  $v$  to  $c$  transitions at individual  $k$ -points. In recent years, it has been found that two-dimensional (2D) layered materials [8, 9] can exhibit very large bulk photovoltaic effects [10] and non-linear optical responses [11–13]; these 2D materials also offer the prospect of bottom-up design through integration with other materials [14, 15] or photonic devices [16, 17]. Due to reduced electronic screening in 2D [18], electron-hole

interactions and hence excitonic effects are more pronounced. It therefore becomes increasingly important to establish an understanding of the shift current within the many-body formalism.

Early attempts to incorporate many-body effects in the shift current description stayed within the IPA to describe the shift current and shift vector [19], incorporating the many-body effects in the components of the IPA expression. A more recent work used a time-dependent GW approach to predict the shift current [20], demonstrating significant excitonic enhancement for the shift current in 2D materials. Using an approximated shift current tensor [20], the authors attributed the shift current enhancement primarily to the effect of enhanced optical absorption due to excitons, and additional non-linear effects from the coupling between excitons. A recent GW-BSE calculation for shift currents in hexagonal boron nitride systems also attributed the observed excitonic-enhancement to the large oscillator strength of the low-lying exciton [21]. However, while the oscillator strengths of some excitations may be increased, oscillator strengths are governed by a sum rule [22], so it is not clear then if shift currents integrated over energies would in general be enhanced by excitons.

We derive an expression for the many-body shift current from time-dependent perturbation theory, using as a basis the exciton states obtained from a first principles GW-BSE approach [7]. This many-body expression reduces to the IPA shift current in the non-interacting limit. The expression allows for a natural definition of

a many-body shift vector which is the dominant contribution to the many-body shift current. We show that strong excitonic effects can significantly enhance the shift currents, and we provide a clear, physically-motivated understanding of this excitonic enhancement, which can be seen to be general for all systems hosting excitons. Specifically, the many-body shift vector arises from positional changes from valence to conduction states, associated with *pairs* of distinct but nearly-degenerate excitons that overlap in reciprocal space. In the IPA limit, the excitons collapse to single  $v$  to  $c$  transitions at individual  $k$ -points, greatly reducing the likelihood of overlap in reciprocal space.

The many-body excitation energies  $E_S \equiv \hbar\Omega_S$  and many-body eigenstates (excitons),  $|S\rangle = \sum_{v\mathbf{c}\mathbf{k}} A_{v\mathbf{c}\mathbf{k}}^S \hat{a}_{\mathbf{c}\mathbf{k}}^\dagger \hat{a}_{v\mathbf{k}} |0\rangle$  [23] ( $\hat{a}_{v\mathbf{k}}, \hat{a}_{\mathbf{c}\mathbf{k}}^\dagger$  are the single particle annihilation and creation operators), are obtained by solving the GW-BSE equation [7]:

$$(\varepsilon_{c\mathbf{k}} - \varepsilon_{v\mathbf{k}})A_{v\mathbf{c}\mathbf{k}}^S + \sum_{v'\mathbf{c}'\mathbf{k}'} K_{v\mathbf{c}\mathbf{k},v'\mathbf{c}'\mathbf{k}'}^{eh} A_{v'\mathbf{c}'\mathbf{k}'}^S = E_S A_{v\mathbf{c}\mathbf{k}}^S \quad (1)$$

$\varepsilon_{n\mathbf{k}}$  are the quasiparticle energies calculated within the GW approximation [24] and  $K_{v\mathbf{c}\mathbf{k},v'\mathbf{c}'\mathbf{k}'}^{eh}$  describes the electron-hole interactions. The shift current conductivities  $\sigma_{\beta\gamma}^\alpha$  are defined by  $j^\alpha = \sum_{\beta\gamma} \sigma_{\beta\gamma}^\alpha E^\beta(t) E^{\gamma}(t)$ , where  $j^\alpha$  is the many-body shift current per unit volume, obtained by treating the light-matter interaction as a perturbation to the many-body Hamiltonian, and taking the expectation value of the velocity operator (see S1 for details). Focusing on linearly polarized incident light, we obtain, for incoming light with frequency  $\omega$ ,

$$\begin{aligned} \sigma_{\beta\beta}^\alpha &= \frac{i\mathcal{C}}{\omega^2} \underbrace{\sum_{SS'} \frac{v_{0S}^\alpha p_{SS'}^\beta p_{S'0}^\beta}{\Omega_S - \Omega_0} \delta(\Omega_{S'} - \Omega_0 - \omega)}_{\text{Term 1}} \\ &\quad - \frac{i\mathcal{C}}{\omega^2} \underbrace{\sum_{\Omega_S \neq \Omega_{S'}} \frac{v_{SS'}^\alpha p_{S'0}^\beta p_{0S}^\beta}{\Omega_{S'} - \Omega_S} \delta(\Omega_{S'} - \Omega_0 - \omega)}_{\text{Term 2}} \\ &\quad + (\omega \leftrightarrow -\omega) \end{aligned} \quad (2)$$

We have suppressed the bra-ket notation (e.g.  $\langle S' | \hat{v}^\alpha | S \rangle \equiv v_{S'S}^\alpha$ ) and  $\mathcal{C} = \frac{2\pi e^3}{m^2 \hbar^2 V_{\text{cryst}}}$  factoring in spin degeneracy. When electron-hole interactions ( $K_{v\mathbf{c}\mathbf{k},v'\mathbf{c}'\mathbf{k}'}^{eh}$ ) are set to zero,  $|S\rangle = \hat{a}_{\mathbf{c}\mathbf{k}}^\dagger \hat{a}_{v\mathbf{k}} |0\rangle$ , i.e., the ‘‘exciton’’ reduces to a transition between Bloch states  $|\psi_{v\mathbf{k}}\rangle$  to  $|\psi_{c\mathbf{k}}\rangle$ . We can show analytically and numerically (S2 and Figure S1) that this reduction gives the IPA shift current conductivity [25], which can be re-expressed through a sum rule [3] in terms of the IPA shift vector  $\mathcal{R}_{nm\mathbf{k}}^\alpha$  [4]:

$$\mathcal{R}_{nm\mathbf{k}}^\alpha = \frac{\partial \phi_{nm\mathbf{k}}}{\partial k^\alpha} + \xi_{nm\mathbf{k}}^\alpha - \xi_{mm\mathbf{k}}^\alpha. \quad (3)$$

Here,  $\xi_{nm\mathbf{k}}^\alpha = i \langle u_{n\mathbf{k}} | \frac{\partial u_{m\mathbf{k}}}{\partial k^\alpha} \rangle$  is the  $\alpha$ -component of the position vector representing the electron’s charge center in state  $n\mathbf{k}$  and  $\phi_{nm}$  denotes the phase of the dipole matrix element. However, this sum rule [3] involves matrix elements between states at individual  $k$ -points, and cannot be generalized to matrix elements between many-body states.

The many-body shift current (eq. 2) involves transitions from  $|0\rangle$  to  $|S'\rangle$ , from  $|S'\rangle$  to  $|S\rangle$ , and from  $|S\rangle$  back to  $|0\rangle$  (Figure S2). The shift current is dominated by Term 2 (eq. 2) when  $(\Omega_{S'} - \Omega_S)$  is small. (See S3 for a discussion on numerical considerations related to a physically-motivated broadening of the excitation peaks.) We identify in Term 2

$$\frac{v_{S'S}^\alpha}{i(\Omega_{S'} - \Omega_S)} \equiv r_{S'S}^\alpha, \quad (4)$$

where  $\Omega_{S'} \neq \Omega_S$  and

$$\begin{aligned} r_{S'S}^\alpha &= \underbrace{\sum_{\substack{v\mathbf{k} \\ c \neq c'}} A_{v\mathbf{c}'\mathbf{k}}^{S'*} A_{v\mathbf{c}\mathbf{k}}^S \xi_{c'\mathbf{c}\mathbf{k}}^\alpha - \sum_{\substack{c\mathbf{k} \\ v \neq v'}} A_{v'\mathbf{c}\mathbf{k}}^{S'*} A_{v\mathbf{c}\mathbf{k}}^S \xi_{vv'\mathbf{k}}^\alpha}_{\text{Part a}} \\ &\quad + \underbrace{\sum_{v\mathbf{c}\mathbf{k}} A_{v\mathbf{c}\mathbf{k}}^{S'*} A_{v\mathbf{c}\mathbf{k}}^S (\xi_{c\mathbf{c}\mathbf{k}}^\alpha - \xi_{v\mathbf{v}\mathbf{k}}^\alpha) + i A_{v\mathbf{c}\mathbf{k}}^{S'*} \frac{\partial A_{v\mathbf{c}\mathbf{k}}^S}{\partial k_v^\alpha} - i A_{v\mathbf{c}\mathbf{k}}^S \frac{\partial A_{v\mathbf{c}\mathbf{k}}^{S'*}}{\partial k_c^\alpha}}_{\text{Part b}} \end{aligned} \quad (5)$$

This expression has a structure reminiscent of the IPA shift vector (eq. 3). Part b is the closest analogue; the second and third terms in b ensure gauge invariance similar to  $\frac{\partial \phi_{nm}(\mathbf{k})}{\partial k^\alpha}$  in eq. 3 (see S4).

We now apply our formalism to bulk BaTiO<sub>3</sub> [28] (see S5 for computational details). Figure 1(a) shows that the many-body shift current agrees better with experiment [26, 27] than the IPA shift current computed using the GW quasiparticle energies. Term 1, which is not associated with the many-body shift vector, contributes a small but non-negligible current (Figure 1(b)). Term 2 dominates the shift current and Terms 2a and 2b, arising from Parts a and b of the shift vector, are comparable in magnitude, but not necessarily in the same direction (Figure 1(c-d)).

We plot in Figure 2 the shift current conductivities  $\sigma$  for BaTiO<sub>3</sub>, monolayer NbOCl<sub>2</sub> and monolayer MoS<sub>2</sub>. For all three systems, the many-body shift current arises primarily from Term 2 (the shift vector term), and predominantly from contributions due to *nearly*-degenerate excitons  $S$  and  $S'$  (Figure 2; red dashed lines include only contributions from excitons with energies differing by 0.5 eV or less). Motivated by the form of Term 2 in Eq. 2, we define  $\delta^{\text{n-d}}$  (plotted in green in Figure 2) as:

$$\delta_\alpha^{\text{n-d}}(\Omega'_S) = \frac{1}{V_{\text{cryst}}} \sum_{\substack{|\Omega_S - \Omega_{S'}| \leq 0.5, \\ \Omega_S \neq \Omega_{S'}}} \delta(\Omega_S - \Omega_{S'}) |p_{0S}^\alpha| |p_{S'0}^\alpha|. \quad (6)$$

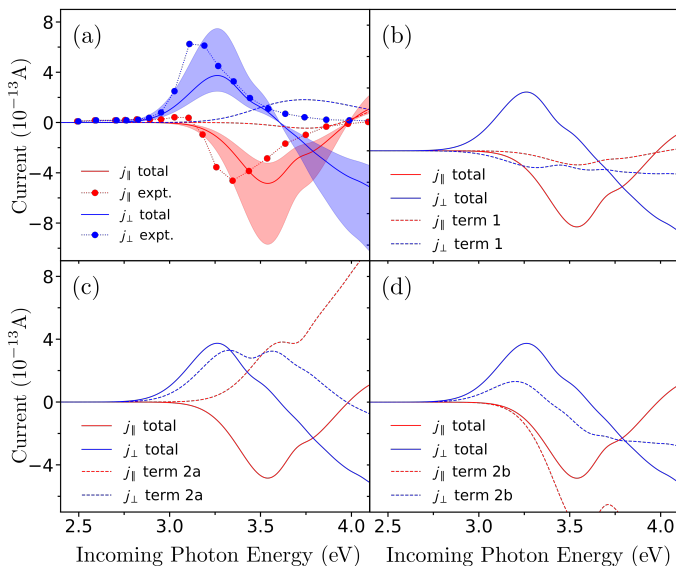


FIG. 1. Shift current in BaTiO<sub>3</sub>. (a) Comparison of the calculated many-body (GW-BSE) shift current with experiment [26, 27]. The shift current (solid lines) is computed using a set of experimental parameters (see S5), and the shaded region represents the expected variation in the shift current for the full range of experimental parameters presented in [26, 27]. The calculated GW-IPA shift current spectrum is in dashed lines for comparison. (b)-(d) Decomposition of the total calculated shift current, showing the contribution arising from Terms (b) 1, (c) 2a, and (d) 2b.

$\delta^{n-d}$  is relatively easy to compute and can predict reasonably well the peak positions of the shift current conductivities (Figure 2). Broadly speaking, we expect large  $|\sigma|$  for incoming photon energies where there is a high density of nearly degenerate optically-active excitons, because this is associated with a large many-body shift vector magnitude,  $|\mathbf{r}_{SS'}$ .

We also see that excitonic effects not only change the qualitative shape of the  $\sigma$  spectra, but also enhance  $|\sigma|$ , by orders of magnitude for the 2D systems, and less so for bulk BaTiO<sub>3</sub> (Figure 2). The increased excitonic enhancement for 2D systems cannot be explained by  $\delta^{n-d}$ , as the overall magnitudes of  $\delta^{n-d}$  are not significantly different across the three systems. We also point out that this *order-of-magnitude* enhancement in the non-linear response of 2D materials, is not seen in the linear response (see Figure S5 for the linear optical absorption spectra with and without electron-hole interactions). Thus, the excitonic enhancement of shift currents in these systems cannot be attributed to similar enhancement in the linear absorption spectra, in contrast to Ref. [20, 21].

The many-body shift vector involves *pairs* of non-degenerate excitons overlapping in  $k$ -space, with shifts in charge centres arising from the inter-band transitions that are embedded in the many-body correlated electron-hole states (eq. 5). In Figure 3(a), we plot the many-body shift vector (Parts a and b) arising from a particular

pair of excitons in NbOCl<sub>2</sub>. The many-body shift vector arises from the  $k$ -space overlap between the excitons (Figure 3(b-c)). In contrast, the IPA shift vector involves shifts in charge-centres from *individual*  $v$  to  $c$  transitions at specific  $k$ -points. But, noting that the many-body shift current reduces to the IPA expression in the IPA limit, we can use the lens of the many-body formalism to provide new insights into the IPA shift current. Figure 4(a-b) shows excitons with Gaussian envelope functions centered at the same (a) and different (b)  $k$ -points, overlapping in  $k$ -space. In the IPA, the excitons collapse to a single  $k$ -point, corresponding to momentum-direct optical transitions between Bloch states with definite  $k$  (Figure 4(c-d)). Thus, most of the exciton pairs contributing in the many-body picture due to  $k$ -space overlap would not contribute in the IPA (Figure 4(d)). We also note that the overlap results in a non-zero contribution in the IPA limit only for Part a of the many-body shift vector (eq. 5). Part b, with  $v$  and  $c$  being the same for both excitons, vanishes in the IPA limit due to the condition of non-degeneracy. Numerically, we see that the number of  $|\mathbf{p}_{SS'}|$  that are exactly zero is several orders of magnitude larger in the IPA limit compared to the BSE (many-body) case (Figure 2(d)) while the spread in  $|\mathbf{p}_{SS'}|$  is not significantly different.

The IPA limit is the extreme limit in which optical transitions between Bloch states involve single  $k$ -points, resulting in much smaller probabilities of  $k$ -space overlap between transitions. For bulk systems like BaTiO<sub>3</sub> where excitonic effects are present, but screened, the less tightly-bound excitons are more spread out in real space, and thus more localized in reciprocal space, compared to those in layered 2D materials (Figure S7). Thus, the  $k$ -space overlap between excitons is reduced, resulting in a larger proportion of vanishing  $|\mathbf{p}_{SS'}|$  (Figure 2(d)). The matrix elements,  $|\mathbf{p}_{SS'}|$ , can be found in the expressions for general non-linear optical susceptibilities in the many-body formalism [29, 30], and this simple picture predicts that strong excitonic effects can enhance not just the shift current conductivities but also the general non-linear optical response.

We have shown that strong electron-hole interactions can enhance the shift current; it is helpful to recall that the shift current is defined as an expectation value of velocity, and unlike a ballistic current, does not require free carriers [31]. Indeed, even within the excitonic picture, the shift current is governed by a shift in charge centers, which will take place across the region of the sample that is irradiated. We predict that shift currents for bulk photovoltaics can be enhanced by choosing inversion-symmetry breaking layered 2D or quasi-2D systems with strong electron-hole interactions, and a high density of nearly-degenerate excitons optically active in the solar spectrum.

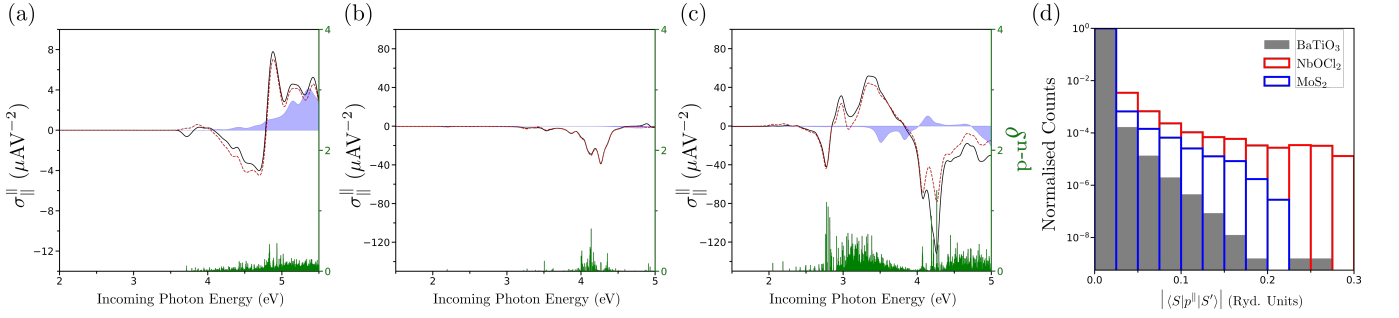


FIG. 2. Shift current conductivities computed with GW-BSE (black curves) and GW-IPA (blue shaded region) for (a) BaTiO<sub>3</sub>, (b) monolayer NbOCl<sub>2</sub>, (c) monolayer MoS<sub>2</sub>, and (d) distribution of  $|\langle S|p||S'\rangle|$  for pairs of nearly degenerate excitons contributing to the red dashed lines in (a-c).  $\parallel$  and  $\perp$  refer to directions parallel to and perpendicular to the polar directions in BaTiO<sub>3</sub> and NbOCl<sub>2</sub>. For MoS<sub>2</sub>, the shift current conductivity is reported in the armchair direction. Red dashed curves are the shift currents from nearly-degenerate exciton pairs (see text). Green vertical bars (right axis) denote the density of nearly-degenerate (n-d) excitons, weighted by the product of the magnitudes of the oscillator strengths of both excitons ( $\delta^{n-d}$  - see text). The GW-IPA shift current conductivity is very small for NbOCl<sub>2</sub> and is seen as a faint blue line in (b). Atomic structures, band structures and linear optical absorption spectra are shown in Figures S3-S5. (d) Distribution of  $|\langle S|p||S'\rangle|$ , where  $\parallel$  is along the axis of the shift current, for pairs of nearly degenerate excitons in BaTiO<sub>3</sub>, NbOCl<sub>2</sub> and MoS<sub>2</sub> contributing to the red dashed lines in (a-c).

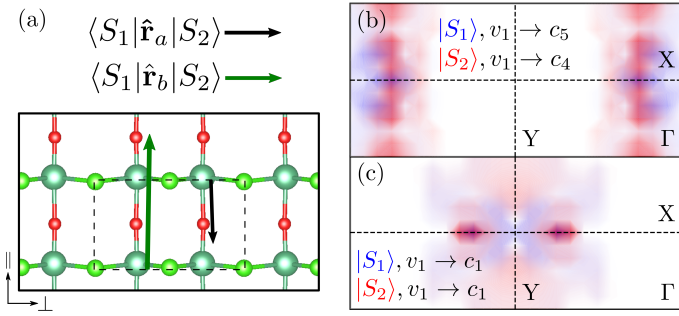


FIG. 3. Many-body shift vector in NbOCl<sub>2</sub>. (a) Parts a and b in equation (5) for excitonic transitions between two excitons,  $S_1$  and  $S_2$ , visualised as a vector in real space (dotted lines: unit cell). (b-c) Overlap in the  $|A_{vck}^S|$  distribution in the Brillouin Zone for (b)  $v_1 \rightarrow c_5$  band for exciton  $S_1$  and  $v_1 \rightarrow c_4$  for  $S_2$  and (c)  $v_1 \rightarrow c_1$  for both  $S_1$  and  $S_2$ . The  $k$ -space overlap in (b) and (c) contribute to Parts a and b of the shift vector, respectively.

## ACKNOWLEDGEMENTS

This work is supported by NUS and the National Research Foundation (NRF), Singapore, under the NRF medium-sized centre programme. Calculations were performed on the computational cluster in the Centre for Advanced 2D Materials and the National Supercomputing Centre, Singapore.

\* phyqsy@nus.edu.sg

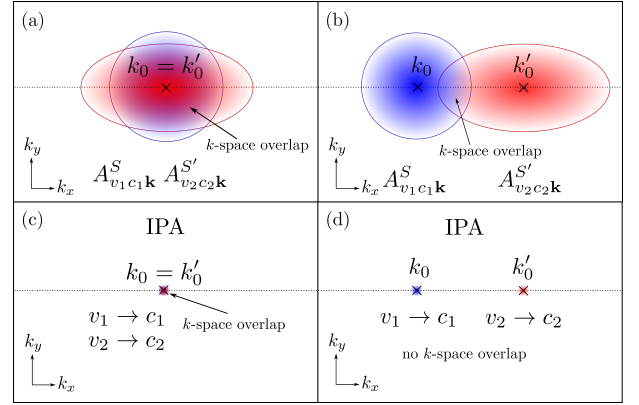


FIG. 4. Schematic illustrating the origin of excitonic enhancement of the many-body shift vector. (a) Two excitons with Gaussian envelope functions centered at the same  $k$ -point. (b) Two excitons with Gaussian envelope functions centered at different  $k$ -points,  $k_0$  and  $k'_0$ . (c-d) The excitons in (a) and (b), respectively, in the IPA limit, where the Gaussian envelope functions collapse to delta functions at  $k_0$  and  $k'_0$ .

- [1] J. E. Spanier, V. M. Fridkin, A. M. Rappe, A. R. Akhshiev, A. Polemi, Y. Qi, Z. Gu, S. M. Young, C. J. Hawley, D. Imbrenda, et al., *Nature Photonics* **10**, 611 (2016).
- [2] W. Kraut and R. von Baltz, *Phys. Rev. B* **19**, 1548 (1979).
- [3] C. Aversa and J.E. Sipe, *Phys. Rev. B* **52**, 14636 (1995).
- [4] J.E. Sipe and A.I. Shkrebtii, *Phys. Rev. B* **61**, 5337 (2000).
- [5] S. M. Young and A. M. Rappe, *Phys. Rev. Lett.* **109**, 116601 (2012).
- [6] A. M. Cook, B. M Fregoso, F. De Juan, S. Coh, and J. E. Moore, *Nature communications* **8**, 1 (2017).
- [7] M. Rohlfling and S. G. Louie, *Phys. Rev. B* **62**, 4927 (2000).

- [8] Y. Jia, M. Zhao, G. Gou, X. C. Zeng, and J. Li, *Nanoscale Horizons* **4**, 1113 (2019).
- [9] C. Wang, L. You, D. Cobden, and J. Wang, *Nature Materials* pp. 1–11 (2023).
- [10] Y. Li, J. Fu, X. Mao, C. Chen, H. Liu, M. Gong, and H. Zeng, *Nature communications* **12**, 5896 (2021).
- [11] I. Abdelwahab, B. Tilmann, Y. Wu, D. Giovanni, I. Verzhbitskiy, M. Zhu, R. Berté, F. Xuan, L. d. S. Menezes, G. Eda, et al., *Nature Photonics* **16**, 644 (2022).
- [12] I. Abdelwahab, B. Tilmann, X. Zhao, I. Verzhbitskiy, R. Berté, G. Eda, W. L. Wilson, G. Grinblat, L. de S. Menezes, K. P. Loh, et al., *Advanced Optical Materials* p. 2202833 (2023).
- [13] Q. Guo, X.-Z. Qi, L. Zhang, M. Gao, S. Hu, W. Zhou, W. Zang, X. Zhao, J. Wang, B. Yan, et al., *Nature* **613**, 53 (2023).
- [14] Z. Qin, Y. Chen, K. Zhu, and Y. Zhao, *ACS Materials Letters* **3**, 1402 (2021).
- [15] U. K. Aryal, M. Ahmadpour, V. Turkovic, H.-G. Rubahn, A. Di Carlo, and M. Madsen, *Nano Energy* **94**, 106833 (2022).
- [16] J. Wu, H. Ma, P. Yin, Y. Ge, Y. Zhang, L. Li, H. Zhang, and H. Lin, *Small Science* **1**, 2000053 (2021).
- [17] Z. Tang, S. Chen, D. Li, X. Wang, and A. Pan, *Journal of Materiomics* **9**, 551 (2023).
- [18] G. Wang, A. Chernikov, M. M. Glazov, T. F. Heinz, X. Marie, T. Amand, and B. Urbaszek, *Rev. Mod. Phys.* **90**, 021001 (2018).
- [19] R. Fei, L. Z. Tan, and A. M. Rappe, *Phys. Rev. B* **101**, 045104 (2020).
- [20] Y.-H. Chan, D. Y. Qiu, F. H. da Jornada, and S. G. Louie, *Proceedings of the National Academy of Sciences* **118**, e1906938118 (2021).
- [21] Y.-S. Huang, Y.-H. Chan, and G.-Y. Guo, *Physical Review B* **108**, 075413 (2023).
- [22] F. Bassani, in *Encyclopedia of Condensed Matter Physics*, edited by F. Bassani, G. L. Liedl, and P. Wyder (Elsevier, Oxford, 2005), pp. 200–206, ISBN 978-0-12-369401-0, URL <https://www.sciencedirect.com/science/article/pii/B012369401900615X>.
- [23] L. X. Benedict, E. L. Shirley, and R. B. Bohn, *Physical review letters* **80**, 4514 (1998).
- [24] M. S. Hybertsen and S. G. Louie, *Phys. Rev. B* **34**, 5390 (1986).
- [25] H. Xu, H. Wang, J. Zhou, and J. Li, *Nature Communications* **12**, 1 (2021).
- [26] W. Koch, R. Munser, W. Ruppel, and P. Würfel, *Solid State Communications* **17**, 847 (1975).
- [27] W. Koch, R. Munser, W. Ruppel, and P. Würfel, *Ferroelectrics* **13**, 305 (1976).
- [28] R. Buttner and E. Maslen, *Acta Crystallographica Section B: Structural Science* **48**, 764 (1992).
- [29] T. G. Pedersen, *Phys. Rev. B* **92**, 235432 (2015).
- [30] F. Xuan, M. Lai, Y. Wu, and S. Y. Quek, *arXiv preprint arXiv:2305.08345* (2023).
- [31] A. M. Burger, R. Agarwal, A. Aprelev, E. Schrubba, A. Gutierrez-Perez, V. M. Fridkin, and J. E. Spanier, *Science advances* **5**, eaau5588 (2019).